Room-temperature five-tesla coercivity of a rare-earth-free shell-ferromagnet

F. Scheibel,[1] D. Spoddig,[1] R. Meckenstock,[1] T. Gottschall,[2] A. Çakır,[1,3] T. Krenke,[4] M. Farle,[1,5] O. Gutfleisch,[2] and M. Acet[1,a)]
[1]*Faculty of Physics, University of Duisburg-Essen, 47057 Duisburg, Germany*
[2]*Department of Materials Science, Technical University of Darmstadt, 64287 Darmstadt, Germany*
[3]*Department of Metallurgical and Materials Engineering, Muğla S itk i Koçman University, 48000 Mugla, Turkey*
[4]*thyssenkrupp Steel Europe AG, Kaiser-Wilhelm-Str. 100, 47166 Duisburg, Germany*
[5]*Center for FunMagMa, Immanuel Kant Baltic Federal University, 236041 Kaliningrad, Russian Federation*

(Received 11 February 2017; accepted 27 April 2017; published online 8 May 2017)

Ni_2MnX-based Heusler (X: main group element), when enriched with Mn, will decompose into ferromagnetic Ni_2MnX and antiferromagnetic NiMn when temper-annealed around 650 K. When the starting material is chosen such that the X-composition is about 5 at. % and the annealing takes place in the presence of a magnetic field of about 1 T, the resulting material is a composite of nanoprecipitate strongly pinned shell-ferromagnets with a soft ferromagnetic core embedded in the antiferromagnetic matrix. We show that the shells of the precipitates are so strongly pinned that the estimated field required to fully reorient the spins is in the order of 20 T. We examine in a $Ni_{50.0}Mn_{45.1}In_{4.9}$ sample the pinning and the magnetic interactions of the precipitate and the matrix with magnetization and ferromagnetic resonance studies carried out in fields ranging up to 14 and 12 T, respectively. *Published by AIP Publishing.* [http://dx.doi.org/10.1063/1.4983199]

Shell-ferromagnetism in Mn-rich antiferromagnetic (AF) Heusler-based compounds is a recently discovered effect that opens paths to possible functionalities.[1] When $Ni_{50}Mn_{45}In_5$ is temper-annealed at temperatures around 600 K in a magnetic field of about 0.1 T, it decomposes and forms nanoprecipitates with a ferromagnetic (FM) shell that is strongly pinned by the AF matrix in which they become embedded. A collection of shell-FM precipitates in a macroscopic sample gives rise to a "monopolar" response to an applied magnetic field.[2] Such strong pinning carries the implication that shell-ferromagnetism could form building blocks for high-performance and light-weight permanent magnets of unsurpassed coercivity at a very cheap price. Here, we show that the coercive field of the shell-FM precipitates exceeds 5 T and that the shell moments can only be fully reoriented in fields exceeding 20 T, all up to 500 K. We undertake magnetization and ferromagnetic resonance (FMR) studies in fields of up to 14 T to examine the strong pinning of the shell-FM effect in detail.

Functionalities based on martensitic phase transitions are encountered in numerous materials. Among them, the Heusler-based compounds contribute with a fair share.[3–6] The phase transformation in Ni-Mn-based Heuslers close to the 2-1-1 stoichiometry is magnetostructural. It occurs around room temperature and involves the strong coupling of ferromagnetic (FM) and antiferromagnetic (AF) interactions to the lattice so that the transition can be driven by mechanical stress or magnetic field and thus be exploited for specially adapted functionalities.[7–9]

Starting with FM Ni_2MnX (X: Ga, In, Sn, and Sb) and gradually substituting Mn for X leads to the strengthening of AF exchange.[10–13] The strongest AF coupling is attained in $Ni_{50}Mn_{50}$. Interestingly, temper-annealing off-stoichiometric $Ni_{50}Mn_{25+x}X_{25-x}$ with $0 < x < 25$ above about 600 K leads to a decomposition towards phases with the $Ni_{50}Mn_{25}X_{25}$ and NiMn stoichiometries.[14,15] On the other hand, temper-annealing at these temperatures, additionally in a magnetic field as little as 0.1 T, can give rise to shell-FM precipitates with a paramagnetic (PM) core. At room temperature, the core becomes a soft ferromagnet. The magnetization of these precipitates can then be not reversed in magnetic fields up to 9 T and at temperatures as high as 500 K. This makes this functional property of Heuslers interesting for non-volatile magnetic data storage and permanent magnet technologies.[1,16,17] A depiction of the shell ferromagnet is given Ref. 1. The depiction is solely for the purpose of the discussions, and its actual form is yet to be determined.

Although the shell-FM model provides a means to describe the behavior of the magnetization, more information is required to understand in detail the magnetic properties of the precipitates. FMR studies at room temperature were previously carried out in fields of ± 0.7 T on non-annealed (as prepared) and in-field decomposed $Ni_{50}Mn_{45}In_5$ to investigate the magnetic coupling at the precipitate/matrix interface and to provide support for the validity of the shell-FM model.[18] It was shown that the FM phase is only present after annealing and that the FMR spectrum is symmetric in forward and reverse field-sweep directions, suggesting that fields at these magnitudes saturate only the loose core-spins of the precipitates and not the pinned, stiff shell-spins. It was not possible in this field-range to detect an effect related to the pinned shell and was concluded that higher fields would be necessary. We therefore investigate here the magnetization and FMR studies of temper-annealed $Ni_{50}Mn_{45}In_5$ in magnetic fields up to 14 T and validate the shell-FM precipitate model.

A $Ni_{50.0}Mn_{45.1}In_{4.9}$ ingot was prepared by arc melting and sealed in a quartz tube under an argon atmosphere. The

a)mehmet.acet@uni-due.de

sample was annealed at 1073 K for 5 days and quenched in ice water. The composition and homogeneity of the sample were investigated by energy dispersive x-ray analysis (EDX). A $1 \times 5 \times 0.8\,\text{mm}^3$ stripe was cut out of the ingot and temper-annealed for 17 h at 650 K and 4.5 T in a furnace attached to a superconducting quantum interference device magnetometer. The magnetization was measured in fields up to 14 T in a commercial vibrating sample magnetometer.

FMR measurements were performed in a home-built setup incorporating a 12 T superconducting magnet accommodated in a temperature-controlled gas-flow cryostat. This technique is based on a resonator system combined with a short of a semi-rigid coaxial cable at one end of the resonator, providing the high-frequency field at the sample position perpendicular to the external filed. The sample is positioned as given in the description in Ref. 19. FMR spectra were obtained at a resonant microwave frequency of 9.048 GHz. The FMR measurements are carried out at 300 K in both field polarities from 0 T to 11.5 T.

Figure 1 shows the field dependence of magnetization $M(B)$ at 300 K and its derivative. $M(B)$ in the range $-14 \le M(B) \le 14$ T in Fig. 1(a) (red curve) is a nearly but not fully closed hysteresis loop as can be seen from the derivative in Fig. 1(b), where $dM(B)/dB$ does not retrace at high fields around ±14 T. $dM(B)/dB$ begins to increase around ±5 T, reaches a maximum around ±8 T, and then gradually drops. If the field is swept only in the range $-5 \le M(B) \le 5$ T, $M(B)$ forms a minor loop (blue curve) as seen in Fig. 1(a) and in the inset for $-1 \le M(B) \le 1$ T, $M(B)$. Therefore, in the absence of very high fields, this minor loop appears as a vertical shift in $M(B)$.[1,16–18]

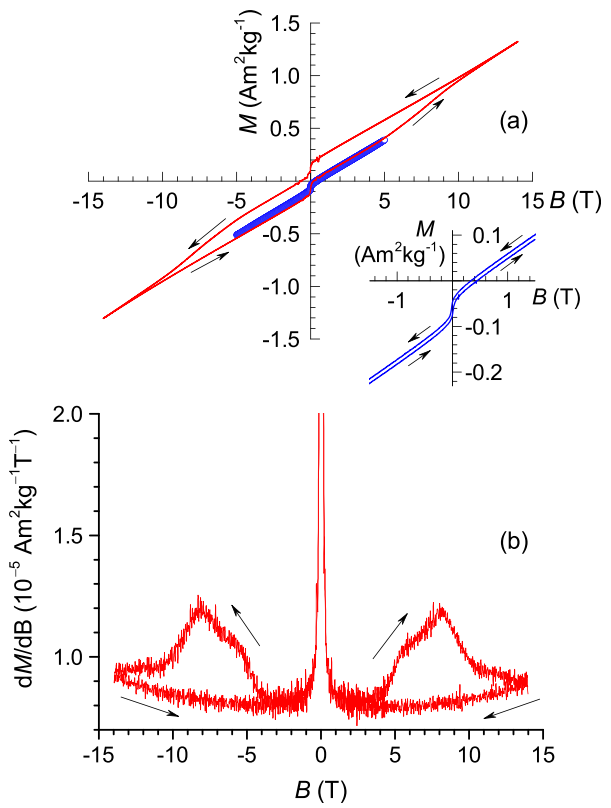

FIG. 1. The magnetization characteristics for $-14 \le M(B) \le 14$ T. The precipitate embedded in the AF matrix has a strongly pinned FM shell and a soft FM core. The paramagnetism of the core is ferromagnetically correlated. Intermediate layers between the shell and the core can also be present. (a) The $M(B)$ loop (red) is nearly symmetric but has a slight positive vertical shift and therefore is a minor loop. The blue curve is a minor loop for $-5 \le M(B) \le 5$ T. The inset shows its details around $-1.5 \le M(B) \le 1.5$ T. (b) $dM(B)/dH$ vs. H shows in more detail the high-field shell-spin rotation. $dM(B)/dH$ does not retrace around high fields of around ±12 T, indicating that the shell-spin rotation is not complete.

The slope of the linear fit to the decreasing-field data of the first quadrant in the range $1 \le M(B) \le 7$ T gives the susceptibility of the AF part with $\chi = 8.19 \times 10^{-6}$ Am^2 kg^{-1}T^{-1}. When the AF contribution is subtracted, a loop related to the ferromagnetism of the precipitate remains (Fig. 2). Even when swept in this high-field range of $-14 \le B \le 14$ T, $M(B)$ follows a minor loop path as seen by the asymmetry around the horizontal axis. A very high coercive field of the precipitate in excess of 5 T is found. The bending of the curve at high-field ends is due to non-linearities in $M(B)$ at these fields and also reflects in the derivative. Nevertheless, it is still possible to extract information on the magnetic properties of the core and the shell. At positive high fields, the core and the shell are aligned. Below about 0.3 T, the magnitude of the soft-core magnetization begins to decrease. At –0.3 T, the change in $M(B)$ with respect to the value at 0.3 T is about 0.136 Am^{2}kg^{-1} so that half of this value is the saturation magnetization of the core, $M_s^{core} = 0.068$ Am^{2}kg^{-1}. What remains at 0 T corresponds to the remanent magnetization at 300 K of the shell attained during the growth of the precipitate; $M_{r+}^{shell} = 0.114$ Am^{2}kg^{-1}, which is also the saturation magnetization of the shell, M_s^{shell}. When the field is reversed to –14 T, the absolute value of the magnetization is smaller than that at +14 T so that the curve is not symmetric about the horizontal axis, and $M_{r-} < M_{r+}$ with $M_{r-}^{shell} = 0.074$ Am^{2}kg^{-1}. However, the change in $M(B)$ between –0.3 T and 0.3 T is again 0.136 Am^{2}kg^{-1} so that $M_s^{core} = 0.068$ Am^{2}kg^{-1} is well determined from both increasing-field and decreasing-field branches.

The saturation magnetization of $Ni_{50}Mn_{25}In_{25}$ is about 75 Am^2 kg^{-1}.[13] Using this value and the saturation magnetization of the precipitate, 0.18 Am^2 kg^{-1} from Fig. 2, we can estimate that the precipitate contributes to the total magnetization by about 0.24%, which is also the volume proportion of the precipitates in the sample. The results of some preliminary transmission electron microscopy and small angle neutron scattering experiments, which will be published elsewhere, suggest that the size of the precipitates is about 2 nm. At this precipitate concentration, 2 nm-precipitates (length of

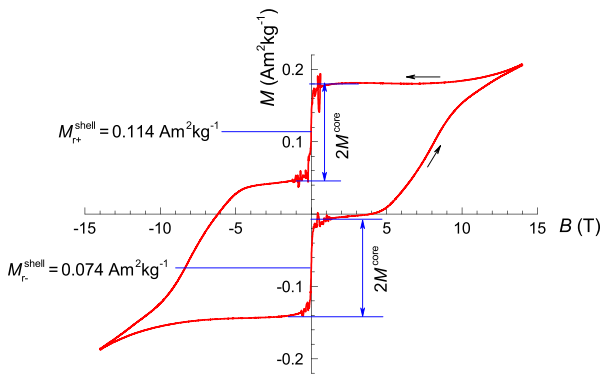

FIG. 2. The extracted magnetization loop of the precipitate. The arrows next to the "core" and "shell" refer to their orientation. The tilted arrows in the lower branches indicate that the rotation is not complete.

about 3–4 Heusler unit cells) would be separated with about 100 nm.

The high-field magnetization loop displays the presence of a hard-pinned shell and a soft FM core. To provide evidence for this picture, we carry out FMR measurements on the same sample by sweeping the field as in the magnetization process. Figure 3 shows the FMR absorption derivative spectra at 300 K for a bidirectional measurement up to 11.5 T. Figure 3(a) shows the spectra in the full range, and Fig. 3(b) shows a magnification for $-1.5 \leq B \leq 1.5$ T.

The sample is mounted with the shell-FM pinning pointing opposite to the initially applied field. Increasing the field saturates the soft FM-core, while the shell remains at the beginning magnetically pinned in the opposite direction. The spectrum also shows an electron paramagnetic resonance (EPR) signal at 0.34 T, which is due to PM surface MnO and does not contribute to the ferromagnetism of the precipitates discussed below. Therefore, the spectrum in the increasing field direction (curve 1, black) exhibits FMR of the soft magnetic core at $B_r = 0.15$ T, close to the field where the core saturates (cf. Fig. 2). Further increasing the field up to 6 T shows no resonance. Above 6 T, the field starts to overcome the coupling of the shell to the surrounding AF matrix, and the magnetization of the shell begins to align with the core. Changes in the dynamical susceptibility in this field-range lead to changes in the absorption derivative as seen in the right-inset of Fig. 3(a). This causes a strongly broadened microwave absorption, which runs differently in the two sweep directions due to its statistical character. Resolving this effect in the resonance requires the contribution of at least 10^8 precipitates. Although the alignment is not full at 11.5 T, the magnetic moments of the atoms of the aligned shells are now in the field direction and contribute to the FMR. As the field is decreased (curve 2, red), FMR appears again at $B_r = 0.15$ T. The intensity of the FMR related to the core is larger in the decreasing-field spectrum since now more spins contribute to the FMR signal being now oriented in the direction of the external field. The same features can be seen when the field is reversed in the negative direction (curve 3, blue; curve 4 green). Resonances appear at negative high fields where the shell spins begin to align with the field [left-inset, Fig. 3(a)], and resonance related to the core appears at $B_r = -0.15$ T. The differences in the intensity of the FMR of the core on increasing and decreasing field branches are due to the different coupling of the core and shell when their magnetic moments align parallel or antiparallel. As seen in the expanded plot in Fig. 3(b), curves 2 and 4 are practically antisymmetric since M_s^{core} is the same in both directions (cf. Fig. 2). However, the integral over the full ± 11.5 T-range of the intensities of these two curves normalized to their respective extrema differs by about 8%, which is in agreement with the minor-loop character of $M(B)$ in Fig. 2. Since curve 1 is a virgin curve, curves 1 and 3 are not antisymmetric. These bidirectional measurements show that the intensity of the FMR depends on the relative amount of parallelly oriented core and shell spins.

To verify the validity of this explanation, we investigated the FMR along a minor loop of ± 2 T. To ensure a defined initial state, the sample was magnetized in -12 T. Figure 4 shows bidirectional FMR spectra starting from $+2$ T since this field is far from any field strong enough to break the antiparallel coupling of the precipitates. Here, we observe that only those precipitates with weak FM coupling, namely, those of the core, contribute to the FMR signal. The EPR signal related to MnO is still present.

The present study first provides validity to the soft FM-core/hard FM-shell nanoprecipitate model for decomposed

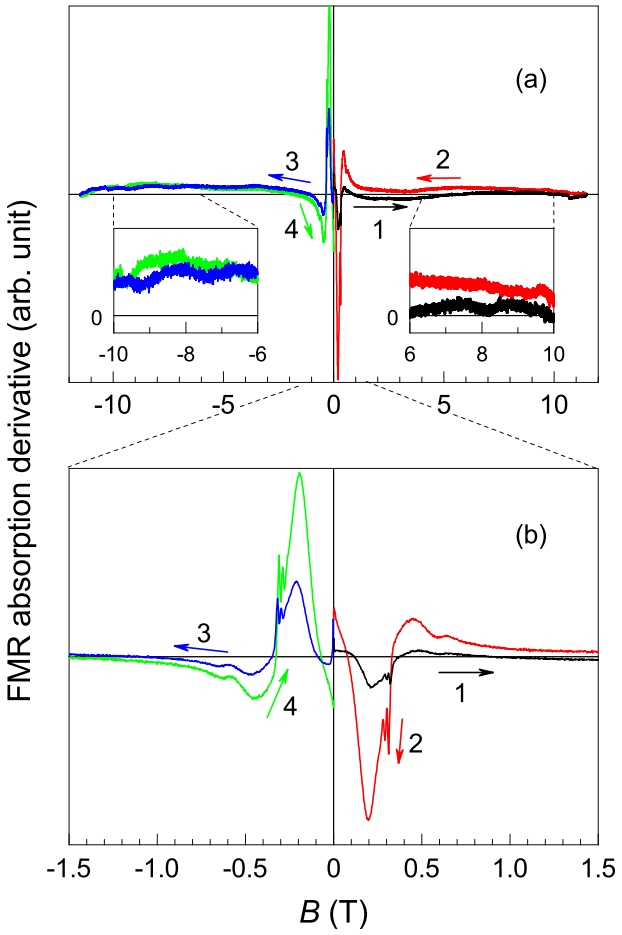

FIG. 3. High-field bidirectional FMR. (a) FMR in the range $-12 \leq B \leq 12$ T. Insets show the details of FMR at high fields related to the rotation of the shell spins. (b) Enlarged area showing the details of the FMR spectra related to the core spins.

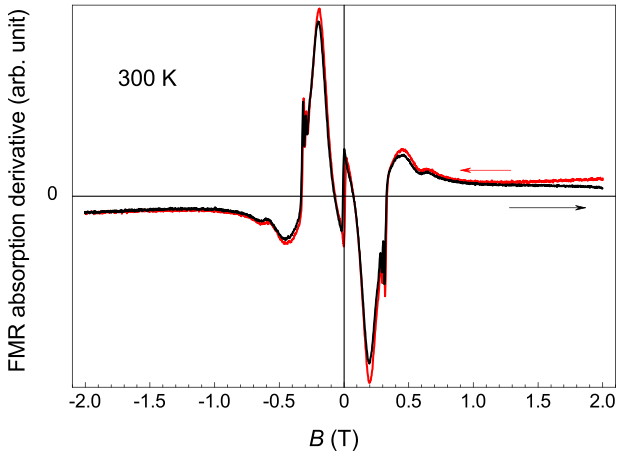

FIG. 4. FMR within a minor loop field-range of $-2 \leq B \leq 2$ T. Resonances related only to the core are observable.

$Ni_{50}Mn_{45}In_5$. Second, an unusually large coercive field of the precipitates in excess of 5 T is striking. There is a big industrially driven interest to design light-weight, rare-earth-free, high performance magnets for electrical power applications, as generators and motors, as well as for magnetic refrigeration. The large coercive field feature can be exploited for their use as permanent magnets composed of relatively cheap and abundant materials and operative at temperatures as high as 500 K. Furthermore, the monopolar response and the capability of adjusting the direction of the anisotropy can also open up possibilities for applications.[20] The material described here and the observed magnetic phenomenon provide a guideline for such possible applications.

This work was supported by the Deutsche Forschungsgemeinschaft (SPP 1599).

[1]A. Cakir, M. Acet, and M. Farle, Sci. Rep. **6**, 28931 (2016).
[2]A. Cakir, https://www.youtube.com/watch?v=0VlSksW2G-s for Shell Ferromagnetism.
[3]K. Ullakko, J. K. Huang, C. Kantner, R. C. O'Handley, and V. V. Kokorin, Appl. Phys. Lett. **69**, 1966 (1996).
[4]A. Planes, L. Mañosa, and M. Acet, J. Phys.: Condens. Matter **21**, 233201 (2009).
[5]I. Dubenko, M. Khan, A. K. Pathak, B. R. Gautam, S. Stadler, N. Ali, and J. Magn, Magn. Mater. **321**, 754 (2009).
[6]C. Felser, L. Wollmann, S. Chadov, G. H. Fecher, and S. S. P. Parkin, APL Mater. **3**, 041518 (2015).
[7]L. Mañosa, D. González-Alonso, A. Planes, E. Bonnot, M. Barrio, J.-L. Tamarit, S. Aksoy, and M. Acet, Nat. Mater. **9**, 478 (2010).
[8]J. Liu, T. Gottschall, K. P. Skokov, J. D. Moore, and O. Gutfleisch, Nat. Mater. **11**, 620 (2012).
[9]M. Acet, L. Mañosa, and A. Planes, in *Handbook of Magnetic Materials*, edited by K. H. J. Buschow (Elsevier, 2011), Vol. 19c, pp. 231–289.
[10]Y. Sutou, Y. Imano, N. Koeda, T. Omori, R. Kainuma, K. Ishida, and K. Oikawa, Appl. Phys. Lett. **85**, 4358 (2004).
[11]S. Aksoy, M. Acet, E. F. Wassermann, T. Krenke, X. Moya, L. Mañosa, A. Planes, and P. P. Deen, Philos. Mag. **89**, 2093–2109 (2009).
[12]T. Krenke, M. Acet, E. F. Wassermann, X. Moya, L. Mañosa, and A. Planes, Phys. Rev. B **72**, 014412 (2005).
[13]T. Krenke, M. Acet, E. F. Wassermann, X. Moya, L. Mañosa, and A. Planes, Phys. Rev. B **73**, 174413 (2006).
[14]D. L. Schlagel, R. W. McCallum, and T. A. Lograsso, J. Alloys Compd. **463**, 38 (2008).
[15]W. M. Yuhasz, D. L. Schlagel, Q. Xing, R. W. McCallum, and T. A. Lograsso, J. Alloys Compd. **492**, 681 (2010).
[16]A. Cakir, M. Acet, U. Wiedwald, T. Krenke, and M. Farle, Acta Mater. **127**, 117 (2017).
[17]T. Krenke, A. Cakir, F. Scheibel, M. Acet, and M. Farle, J. Appl. Phys. **120**, 243904 (2016).
[18]F. Scheibel, D. Spoddig, R. Meckenstock, A. Cakir, M. Farle, and M. Acet, AIP Adv. **7**, 056425 (2017).
[19]F. M. Römer, M. Möller, K. Wagner, L. Gathmann, R. Narkowicz, H. Zähres, B. R. Salles, P. Torelli, R. Meckenstock, J. Lindner, and M. Farle, Appl. Phys. Lett. **100**, 092402 (2016).
[20]A. Cakir, https://www.youtube.com/watch?v=v4OiTxPnSkY for perpendicular anisotropy of a shell ferromagnet.